

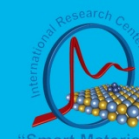
---

**Synchrotron-based experimental study and theoretical simulation of hydrogen desorption for solid-state hydrogen storage material  $\text{Mn}(\text{BH}_4)_2$**   
Ilia A. Pankin, Alexander A. Guda, Vladimir P. Dmitriev, Alexander V. Sodlatov et. al.,  
**IRC "Smart Materials", Rostov-on-Don, Russia**

---



# 1. Motivation

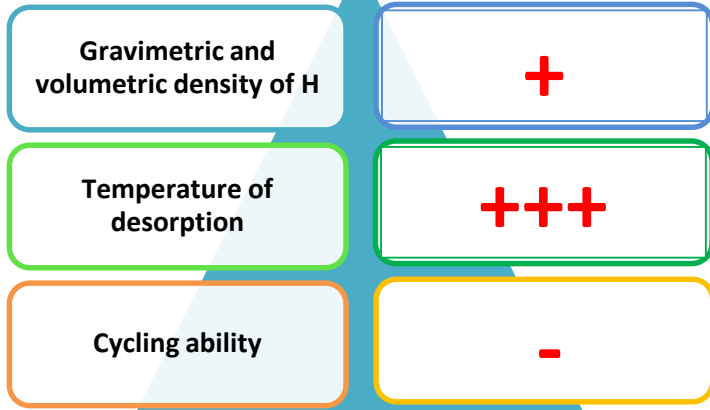


International Research Center  
"Smart Materials"

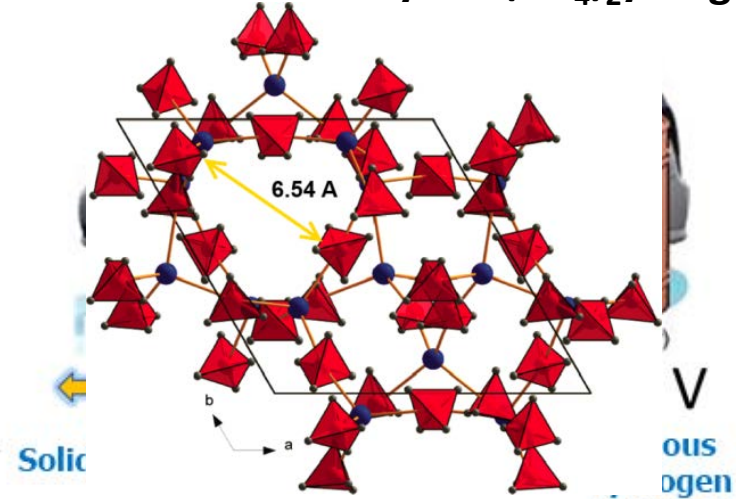


Southern Federal University,  
Rostov-on-Don, Russia

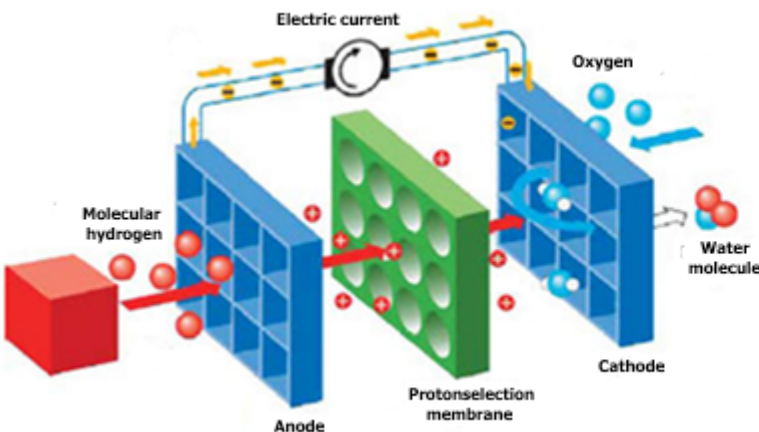
The main requirements:



Compact porous structure of  $Mg(BH_4)_2$  hydrogen!



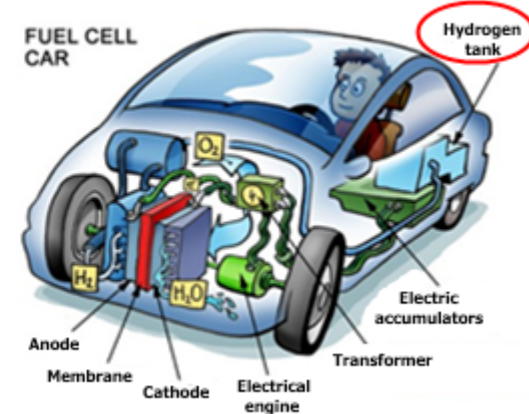
hydrogen fuel cell + solid-state hydrogen storage → breakthrough in mobile applications



Reaction on the anode  
(dissociation of hydrogen molecules):

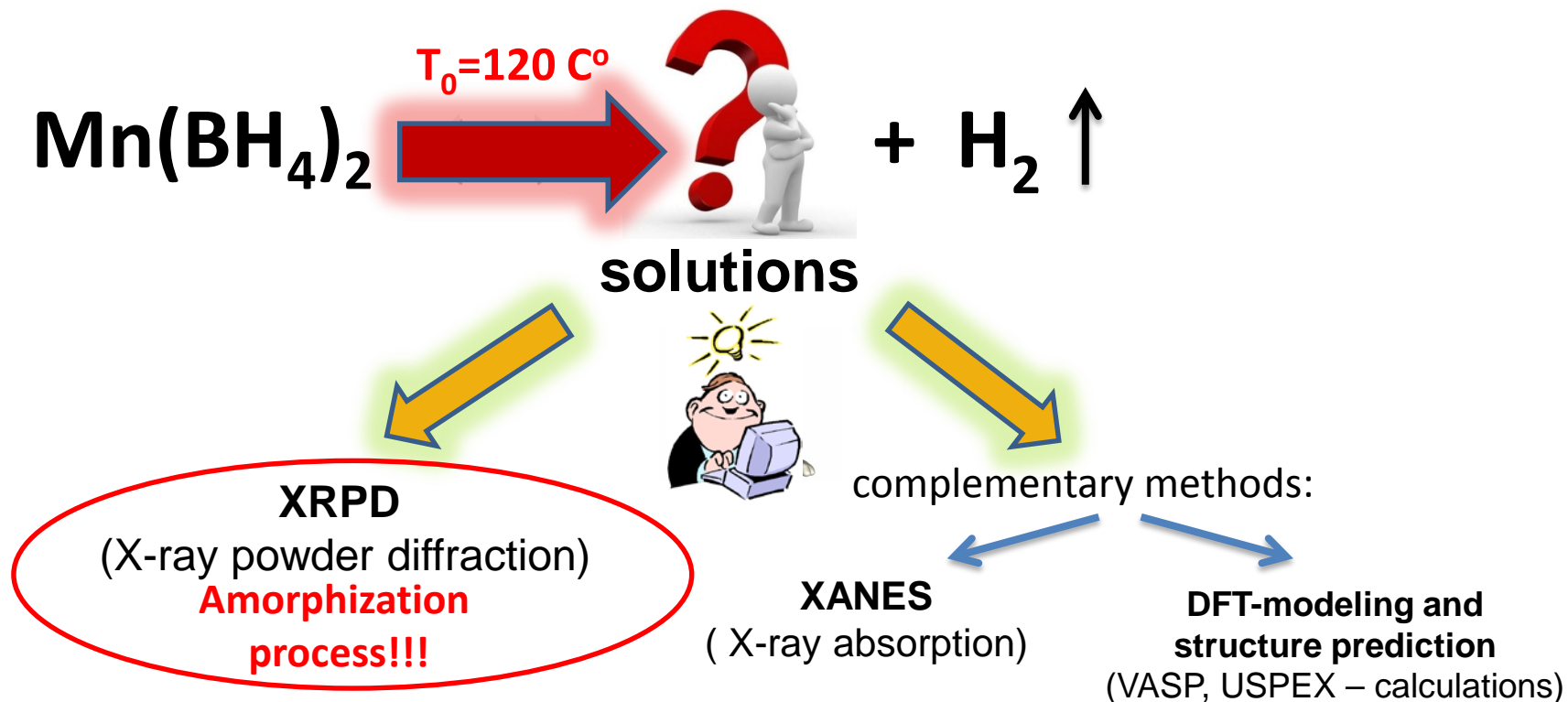


Reaction on the cathode  
(formation of water molecules):

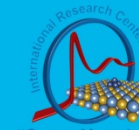


## 2. Purpose of study

General aim – determination of thermal decomposition path.



# 3. XAS spectroscopy



International Research Center  
"Smart Materials"

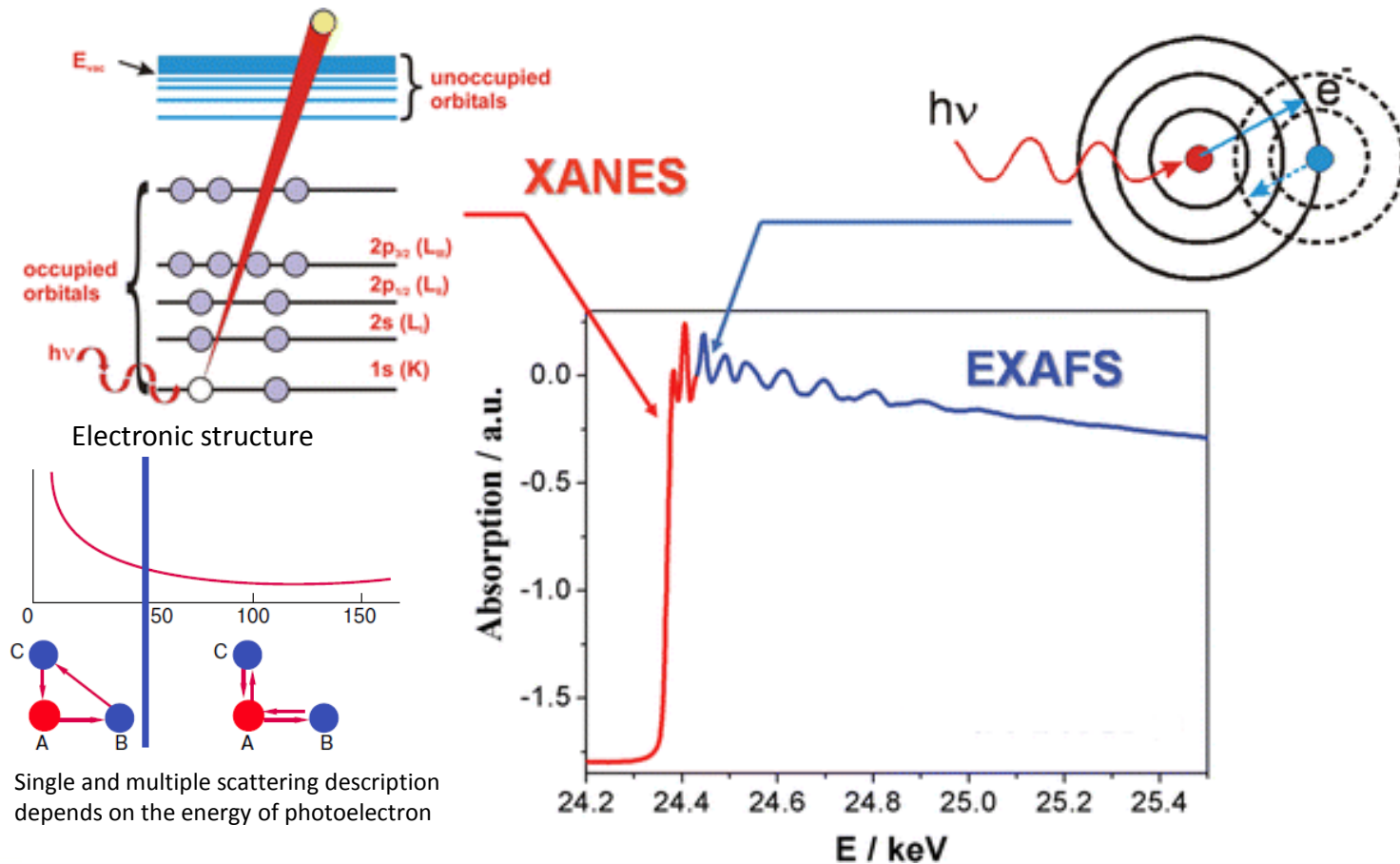


Southern Federal University,  
Rostov-on-Don, Russia

## XAS X-ray Absorption Spectroscopy

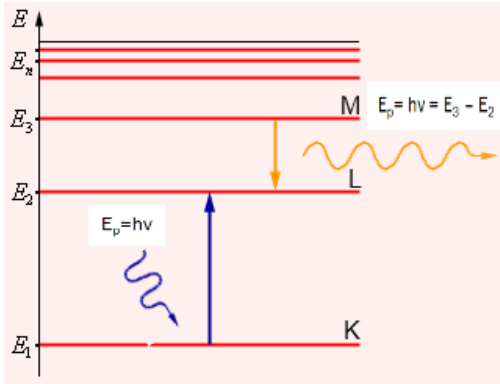
**XANES** X-ray Absorption Near Edge Structure

**EXAFS** Extended X-ray Absorption Fine Structure



# 4. XAS spectroscopy

## Some words about physical background

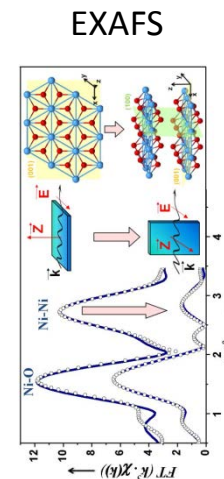
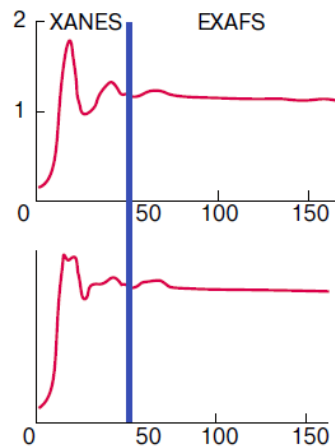
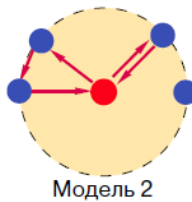
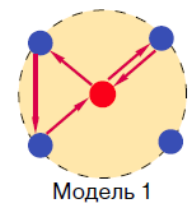


The probability of the electronic transition is determined by density of final states of the system. "Golden Fermi's rule"

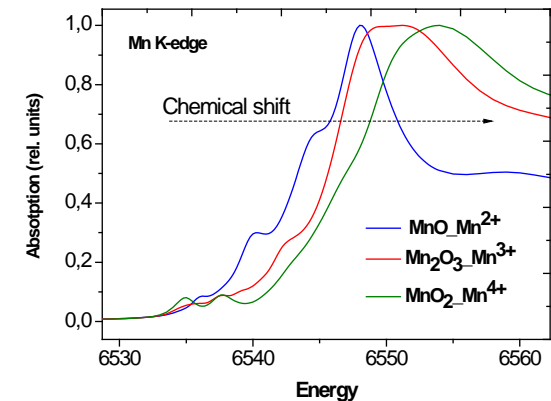
$$W_{i \rightarrow f} = \frac{2\pi}{\hbar} |\langle f | H' | i \rangle|^2 \rho,$$

Density of final state provides information about local atomic and electronic structures, chemical bonding, optical properties and so on.

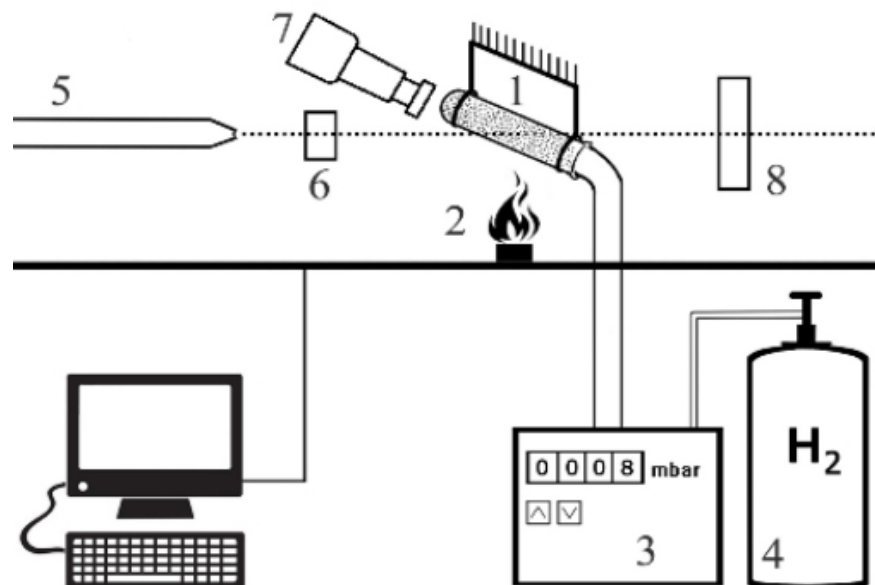
## What information can be extracted?



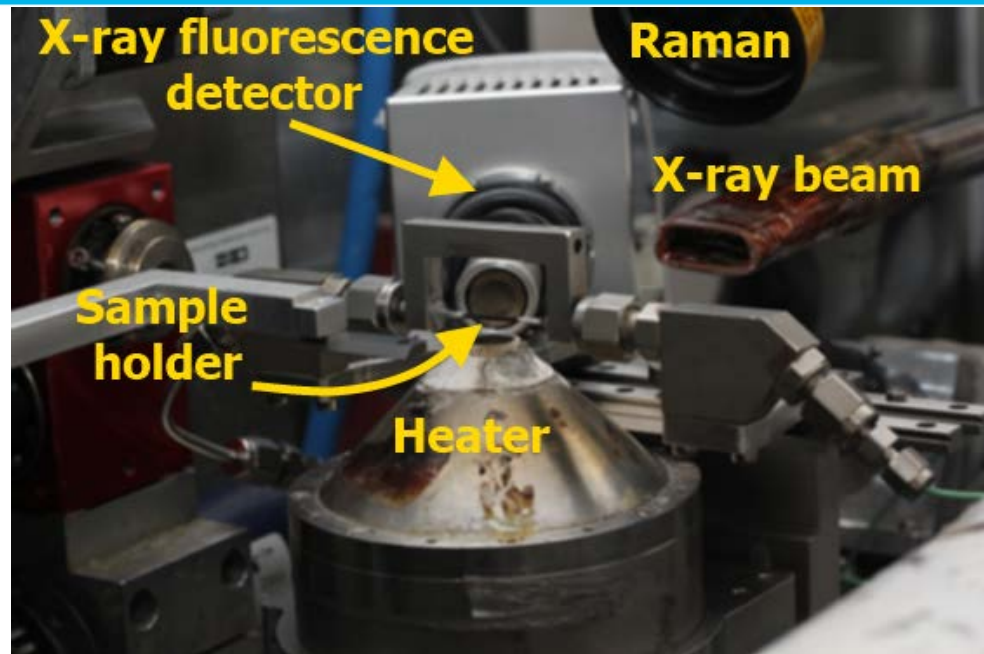
## Oxidation state of absorbing atoms (Chemical shifts)



# 5. Experimental details



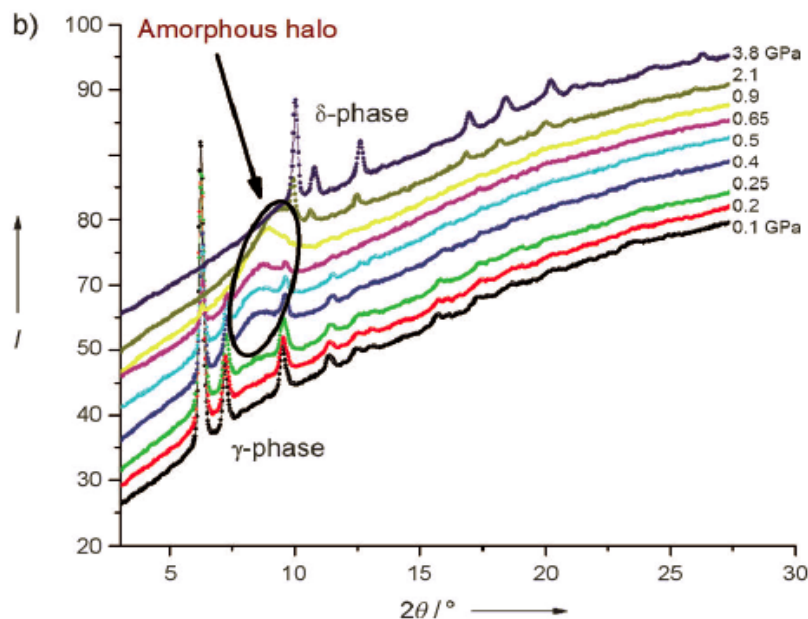
1 - sample holder, 2 - heater, 3 - pressure monitoring system, 4 - hydrogen gas, 5 - X-ray beam, 6 - ionization chamber, 7 - XAS fluorescent detector, 8 XRD detector



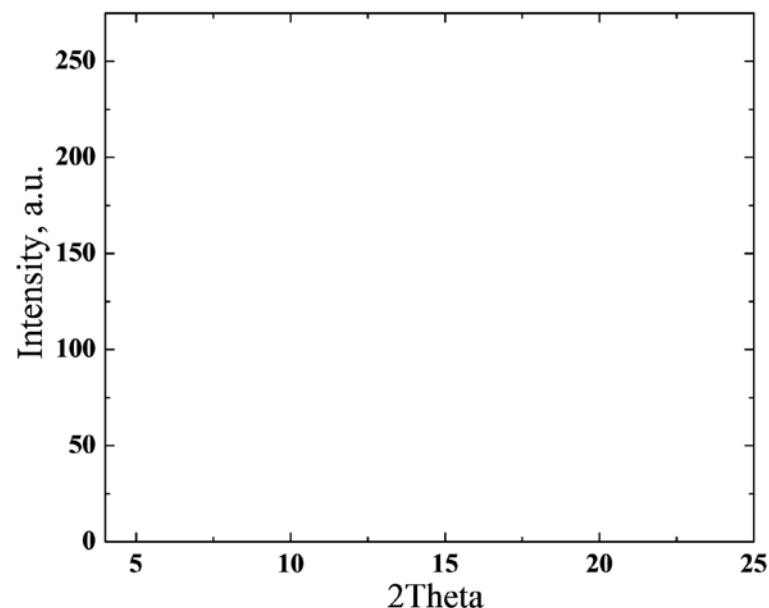
The scheme of the experiment.

# 6. Experimental data

**X-ray powder diffraction** patterns were obtained at different temperature of the sample. Upon heating the significant broadening of diffraction peaks were observed. This tendency corresponds to amorphization of initial material under heating.



Temperature of the sample

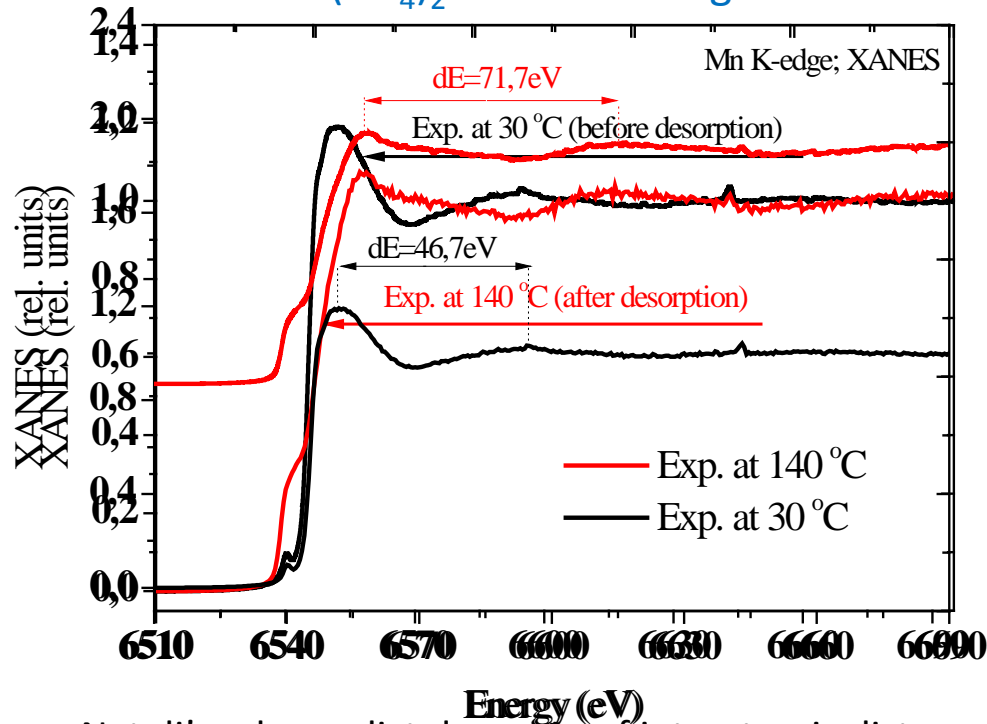


Similar behavior of powder diffraction data for pressure-depends measurements for isomorphous  $\text{Mg}(\text{BH}_4)_2$  was described by Y. Filinchuk et., al.

Y. Filinchuk, B. Richter, T. R. Jensen, V. Dmitriev, D. Chernyshov, and H. Hagemann, *Angewandte Chemie International Edition* 50 (2011) 11162.

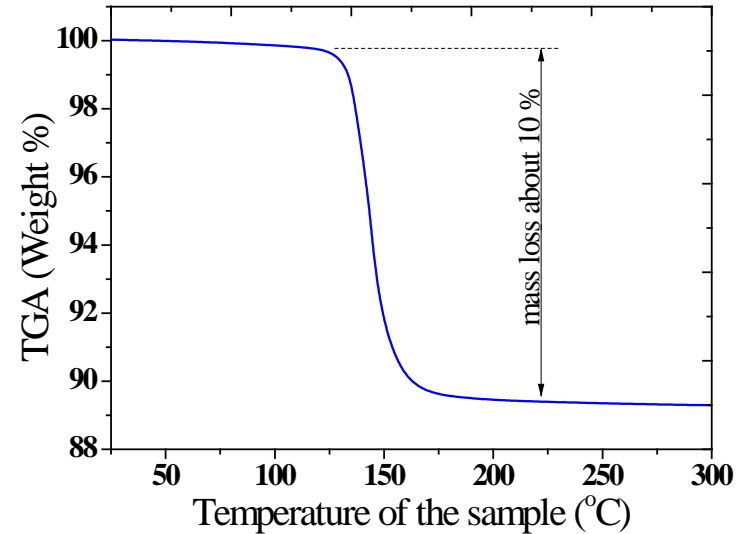
# 7. Experimental data

Evolution of XANES Mn K-edge spectra of  $Mn(BH_4)_2$  under heating.



Natoli's rule predict decrease of interatomic distance  
Mn K-edge spectra of  $Mn(BH_4)_2$  have also undergone  
significant changes after heating the sample.  
 $(E_1 - E_2)R^2 = const$

TGA analysis.



Drastic weight reduction of  $Mn(BH_4)_2$  observed by Cerny et. al. by the mean of TGA analysis. Up to 9,5 % of mass loss were observed at the temperature range from 120 to 160 °C that correspond to the desorption of all hydrogen atoms from the lattice.

We have observed a temperature induced phase transition in  $Mn(BH_4)_2$  which is accompanied by abundant hydrogen release process as well as sample amorphization upon heating!

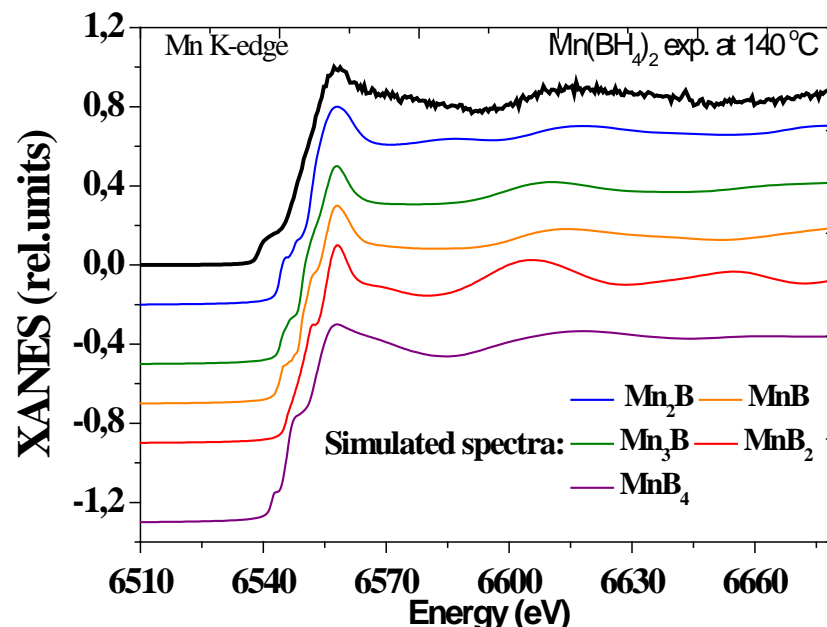
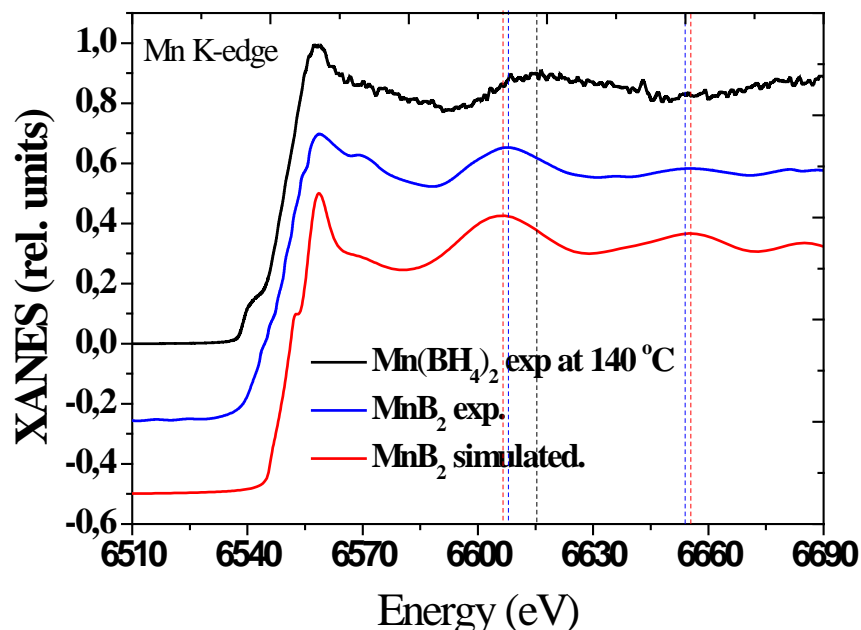




# 8. XANES analysis

The stoichiometry of initial material corresponds to formation of manganese diboride as a possible decomposition reaction product:

$T \uparrow$  hydrogen desorption



Various manganese borides should be taken into account. The spectra calculated for  $\text{Mn}_2\text{B}$ ,  $\text{MnB}$  and  $\text{MnB}_4$  in a good agreement with experimental curve of initial material after heating up to 140 °C.

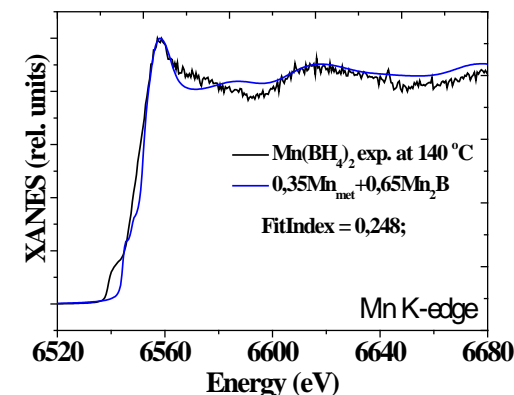
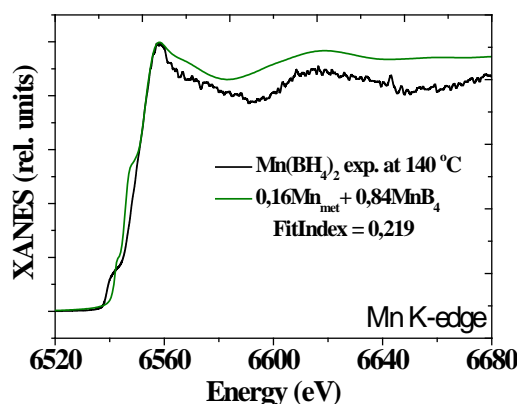
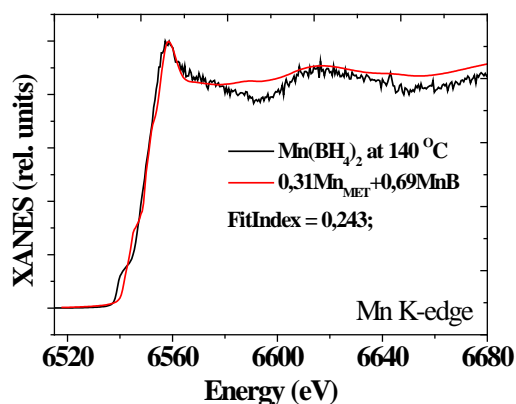
The interatomic distance **Mn-B** and **Mn-Mn** of these borides belong to the range **2,17 - 2,21 Å** and **2,46 - 2,95 Å** respectively compared to **2,44 Å** and **4,80 Å** obtained by XRD data for initial material.

# 9. XANES: Fitting

The most probable decomposition paths obtained from the result of formation enthalpy and Gibbs energy DFT-based calculations\* assume a formation of Mn metallic phase as a possible decomposition product:

$\text{Mn}(\text{BH}_4)_2 \rightarrow \text{Mn} + 2\text{B} + 4\text{H}_2$	(a)
$\text{Mn}(\text{BH}_4)_2 \rightarrow \text{MnH}_2 + 2\text{B} + 3\text{H}_2$	(b)
$\text{Mn}(\text{BH}_4)_2 \rightarrow \text{MnB}_2 + 4\text{H}_2$	(c)
$\text{Mn}(\text{BH}_4)_2 \rightarrow \text{MnH}_2 + \text{B}_2\text{H}_6$	(d)
$\text{Mn}(\text{BH}_4)_2 \rightarrow \text{Mn} + \text{B}_2\text{H}_6 + \text{H}_2$	(e)

A fitting of linear superposition of Mn K-edge XANES spectra for  $\text{Mn}_x\text{B}_y + \text{Mn}_{\text{met}}$  was performed by means of **FitIt** package\*\*.



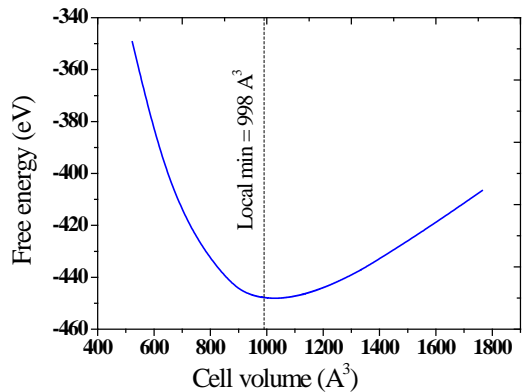
The results of fitting reveal that concentration of metallic Mn phase as a possible decomposition reaction products does not exceed  $30 \pm 5\%$ .

\*Pabitra Choudhury, ‡ Venkat R. Bhethanabotla, \*, †, ‡ and Elias Stefanakos‡, J. Phys. Chem. C 2009 113 (2009) 13416.

\*\*G. Smolentsev, A. V. Soldatov, and M. C. Feiters, Physical Review B 75 (2007) 144106.

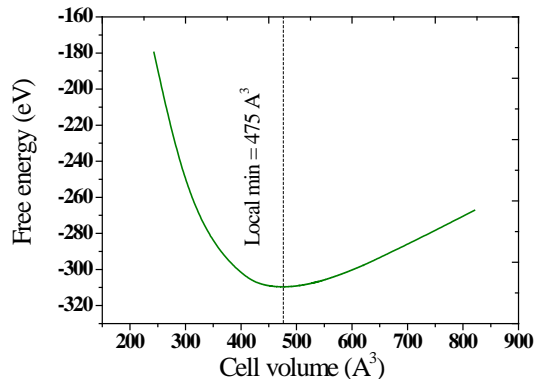
# 10. VASP: DFT modeling

The result of atomic and lattice relaxation: DFT-based modeling (VASP 5.3)



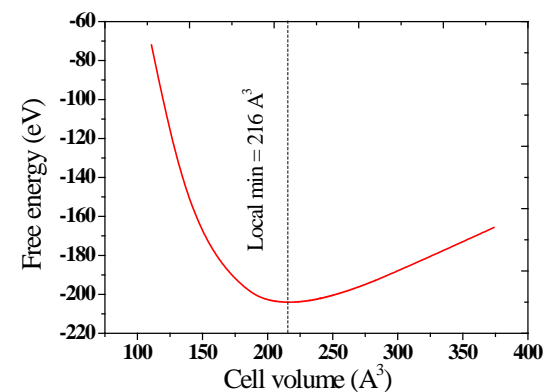
**Model 1:**

Totally occupied hydrogen sites



**Model 2:**

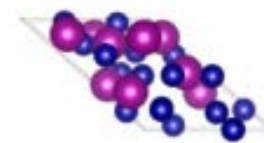
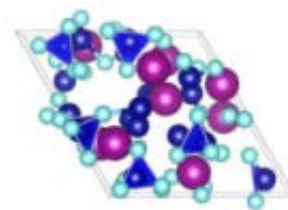
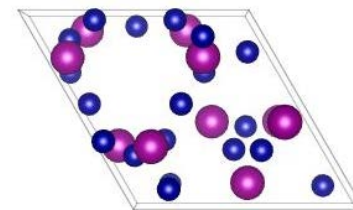
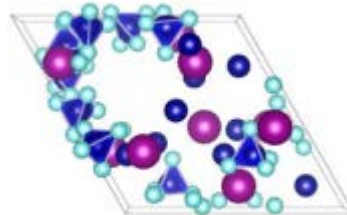
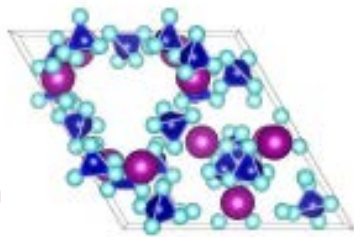
50% of occupied hydrogen sites



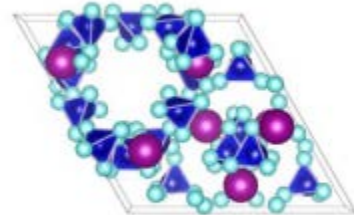
**Model 3:**

Totally unoccupied hydrogen sites

Before  
optimization

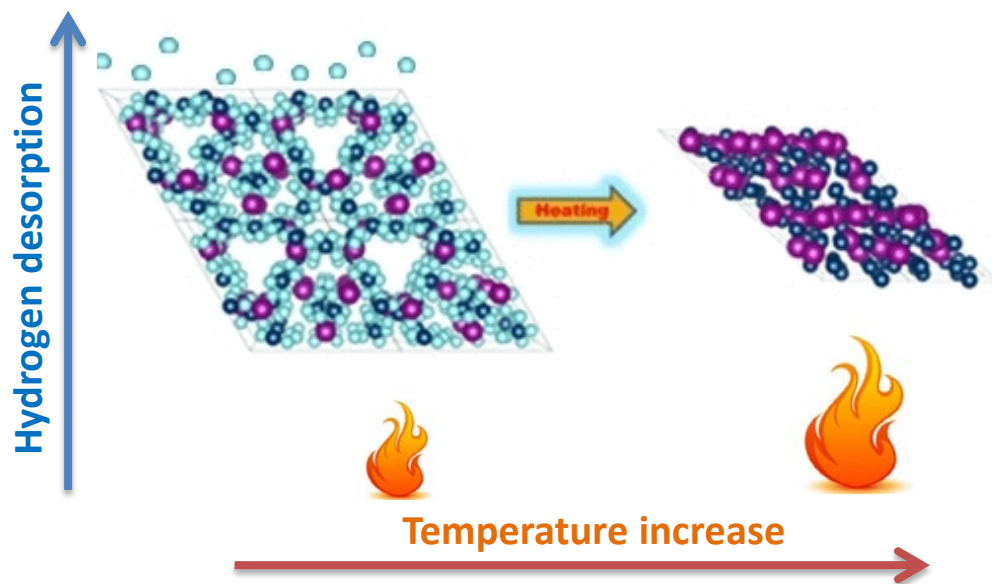
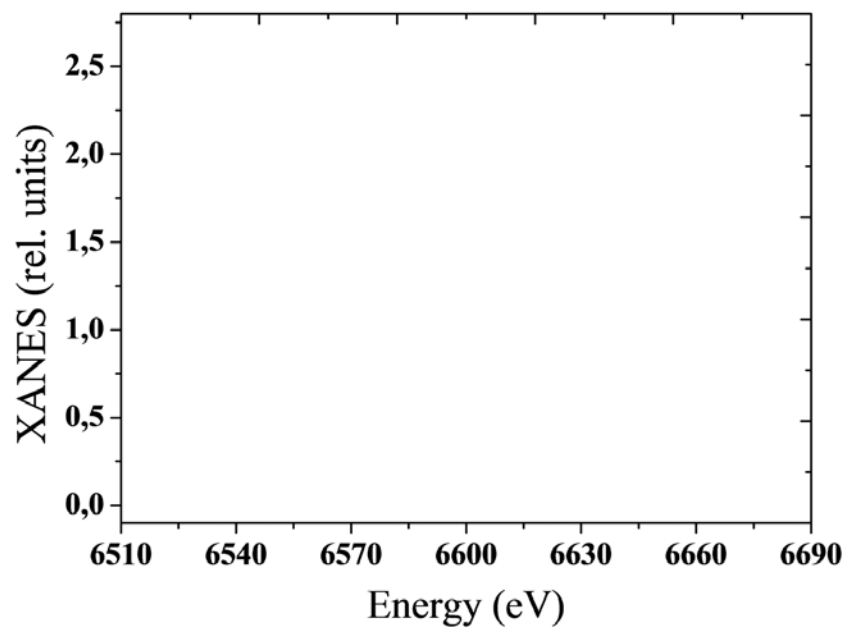


After  
optimization



# 11. XANES analysis

An accuracy of geometry optimization is approved by XANES Mn K-edge spectra calculated for relaxed structural models. Both a difference in the energy localization and ratio of intensity of "white line" for experimental spectra obtained at 30 °C and 140 °C are accurately reproduced at the calculated XANES spectra for models with totally occupied and totally unoccupied hydrogen positions (*model 1* and *model 3*).

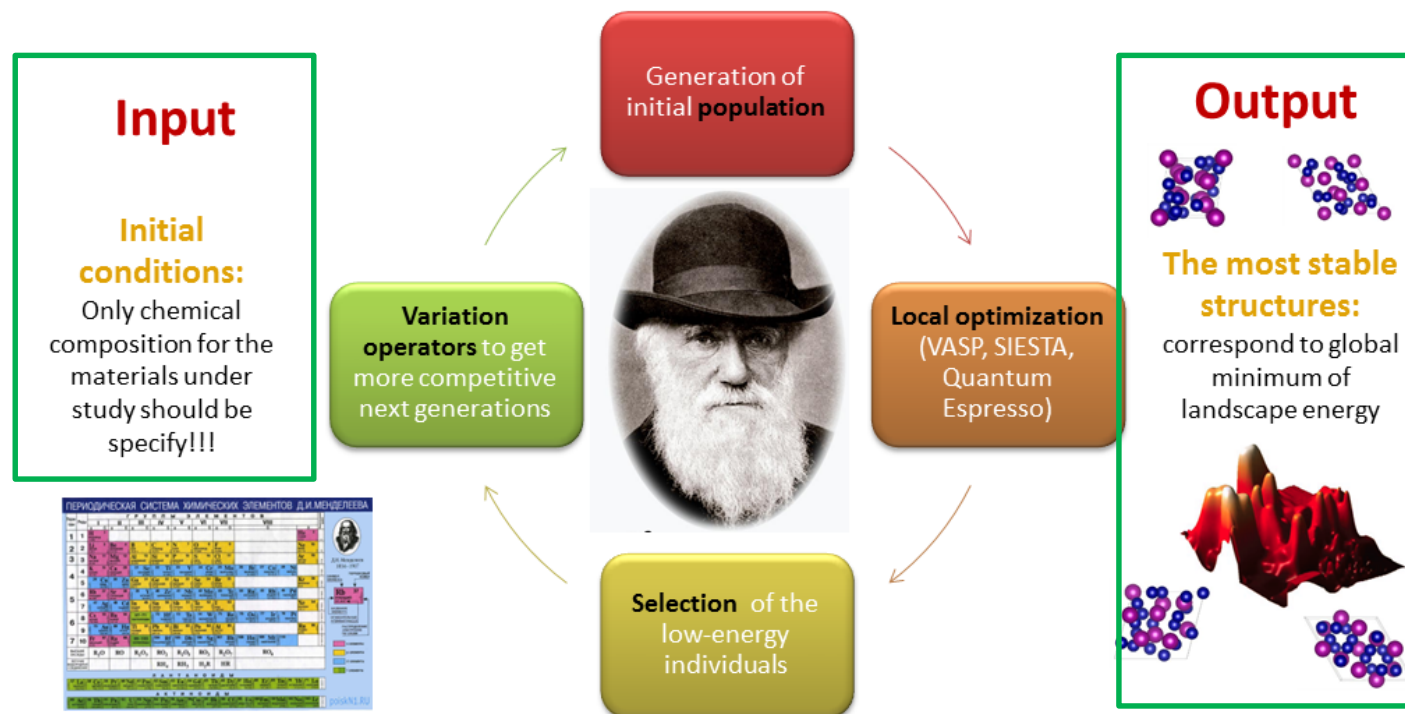


The associative between energy localization of absorption peaks ( $A \rightarrow B, A^* \rightarrow B^*$ ) suggests that interatomic distance Mn-B =  $2,17 \pm 0,05 \text{ \AA}$  and Mn-Mn =  $2,72 \pm 0,18 \text{ \AA}$  have determined correctly.

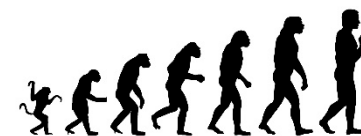
# 12. USPEX: Evolutionary algorithm

## USPEX – Universal Structure Predictor Evolutionary “Xtalography”

Cycle of global minimum searching for multidimensional energy landscape.



Artem Oganov,  
State University of New York  
at Stony Brook, web:  
<http://uspex.stonybrook.edu/uspex.html>



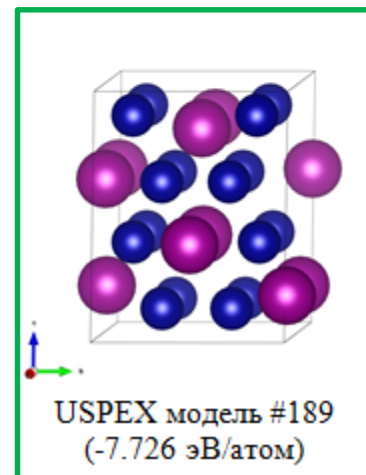
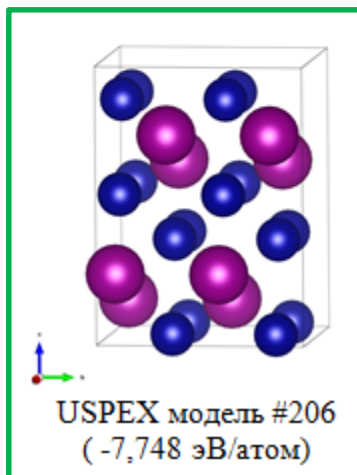
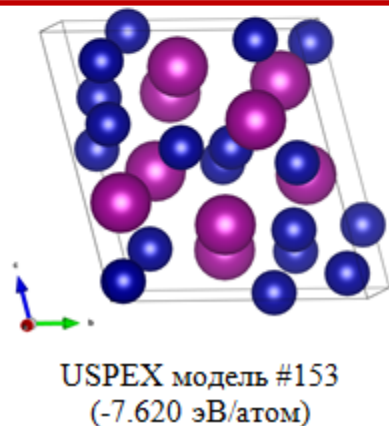
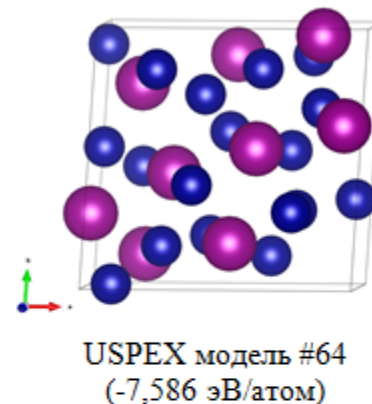
**More about USPEX software:** [1]C. W. Glass, et. al, *Computer Physics Communications* 175 (2006) 713. [2]A.R.Oganov et., al. *the Journal of Chemical Physics* 124 (2006) 244704. [3]A. O. Lyakhov et.al, *Computer Physics Communications* 181 (2010) 1623.



Evolutionary algorithm based on generation of numerous structural models and further selection of the more stable low-energy structures. The revolution idea is AB-initio local optimization and free energy calculation for relaxed structures for each structural models which can be generated randomly, by heredity or lattice mutation and so on.

# 13. USPEX: Evolutionary algorithm

The most stable structural models obtained by USPEX for dense Mn-B system. Structural model obtained by energy minimization with a different amount of hydrogen in **the red box**. The structures with the lower value of free energy obtained by USPEX are **in the green box**.

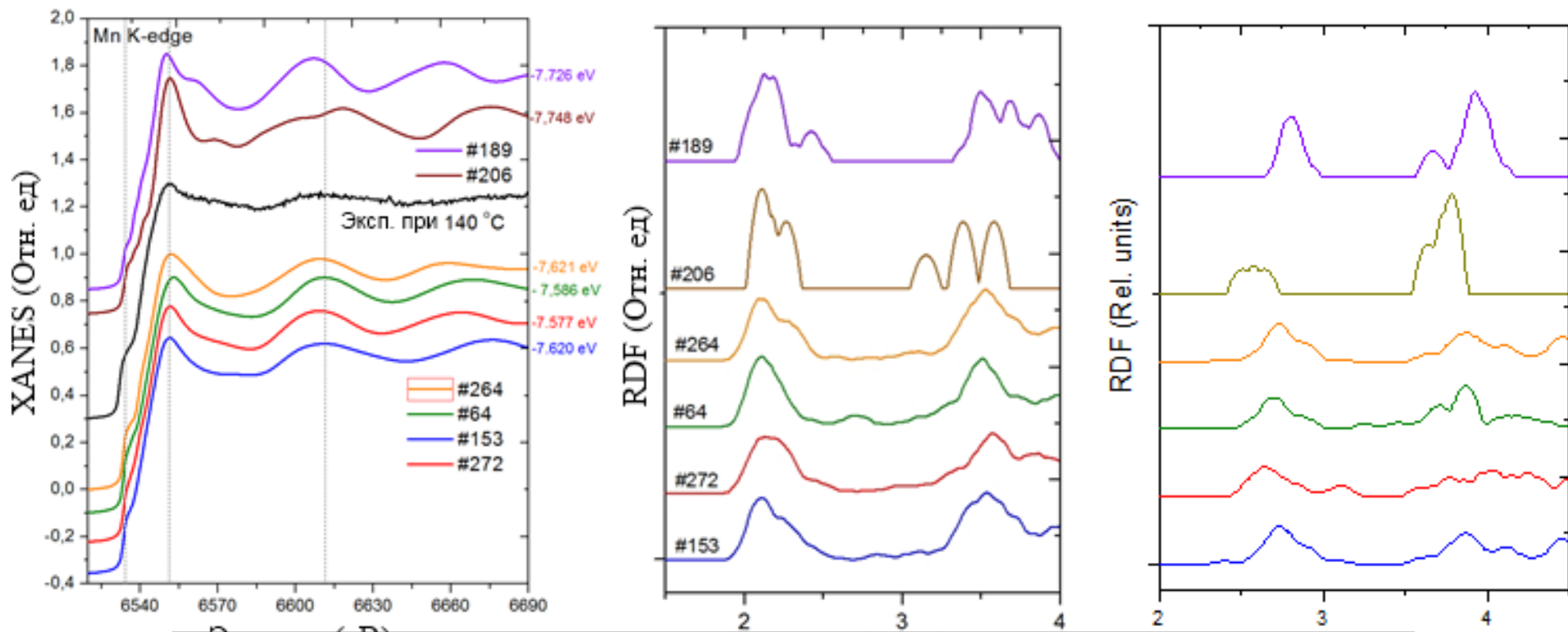


# 14. USPEX: Evolutionary algorithm

Table of structural parameters for the most probable structural models obtained by energy minimization (VASP 5.3 code) and evolutionary algorithm (USPEX code).

Lattice parameters	VASP model 3 $\text{Mn}_9\text{B}_{18}$	USPEX model #264 $\text{Mn}_9\text{B}_{18}$	USPEX model #64 $\text{Mn}_9\text{B}_{18}$	USPEX model #153 $\text{Mn}_9\text{B}_{18}$	USPEX model #206 $\text{Mn}_8\text{B}_{16}$	USPEX model #189 $\text{Mn}_8\text{B}_{16}$
$\vec{a}$ (Å)	5.7853	5.1380	7.5461	5.1523	4.7065	5.5683
$\vec{b}$ (Å)	7.5754	6.4529	7.1143	6.4508	5.2770	5.0069
$\vec{c}$ (Å)	7.5286	6.9740	3.8731	6.9594	7.0625	6.4801
$\alpha$	98.0845	101.2459	92.7232	101.2046	89.9998	90.0015
$\beta$	81.6680	101.4069	83.8648	101.4907	89.9999	102.1064
$\gamma$	138.4502	108.6041	86.5546	108.6317	90.0003	90.0019
$V_{\text{unit cell}}$ (Å <sup>3</sup> )	<b>216.28</b>	<b>206.36</b>	<b>206.06</b>	<b>206.3361</b>	<b>175.41</b>	<b>176.65</b>
Группа симметрии	P 1	P 1	P 1	P 1	<b>C 2/m 2/c 21/m (63)</b>	<b>P 1 21/m 1 (11)</b>
Энтальпия/Атом (Эв)	<b>-7,776</b>	-7,621	- 7,586	-7.620	<b>-7,748</b>	<b>-7,586</b>
Плотность (г/см <sup>3</sup> )	5.290	5.545	5.553	5.545	5.798	5.757

# 15. XANES + RDF modeling



XANES  
agreement  
symmetry  
spheres

Model	Mn-B distance (Å)	Mn-Mn distance (Å)	Cell volume
XRD. Mn(BH <sub>4</sub> ) <sub>2</sub> before heating	2,44 ± 0,02	4,81 - 0,01	1021,7
VASP. Before desorption (Model 1)	2,41 ± 0,01	4,77 ± 0,02	996,8
VASP. Partial desorption (Model 2)	2,28 ± 0,09	3,88 ± 0,24	643,6
VASP. After desorption (Model 3)	2,17 ± 0,05	2,72 ± 0,18	216,3
USPEX	2,08 - 2,14	2,59 - 2,88	206,4

-Mn)  
the best  
at space  
ordination



# 14. Conclusions

1) **X-ray powder diffraction** in combination with **TGA analysis** indicate that process of material amorphization under heating is accompanied by abundant hydrogen release. XANES spectra also undergo significant changes upon heating the sample.

2) **XANES** analysis in combination with AB-initio DFT-based structural modelling represent an powerful equipment of the local atomic structure investigation for the nanoscale and amorphous materials.

3) The result of **geometry optimization** reveals collapse of porous structure as well as amorphization process after the hydrogen atoms were partially or totally removed from the structure.

4) **Significant** decrease of **Mn-B** and especially **Mn-Mn** interatomic distances were obtained from AB-initio DFT modelling upon hydrogen release. It is a good confirmation of Natoli's rule prediction.

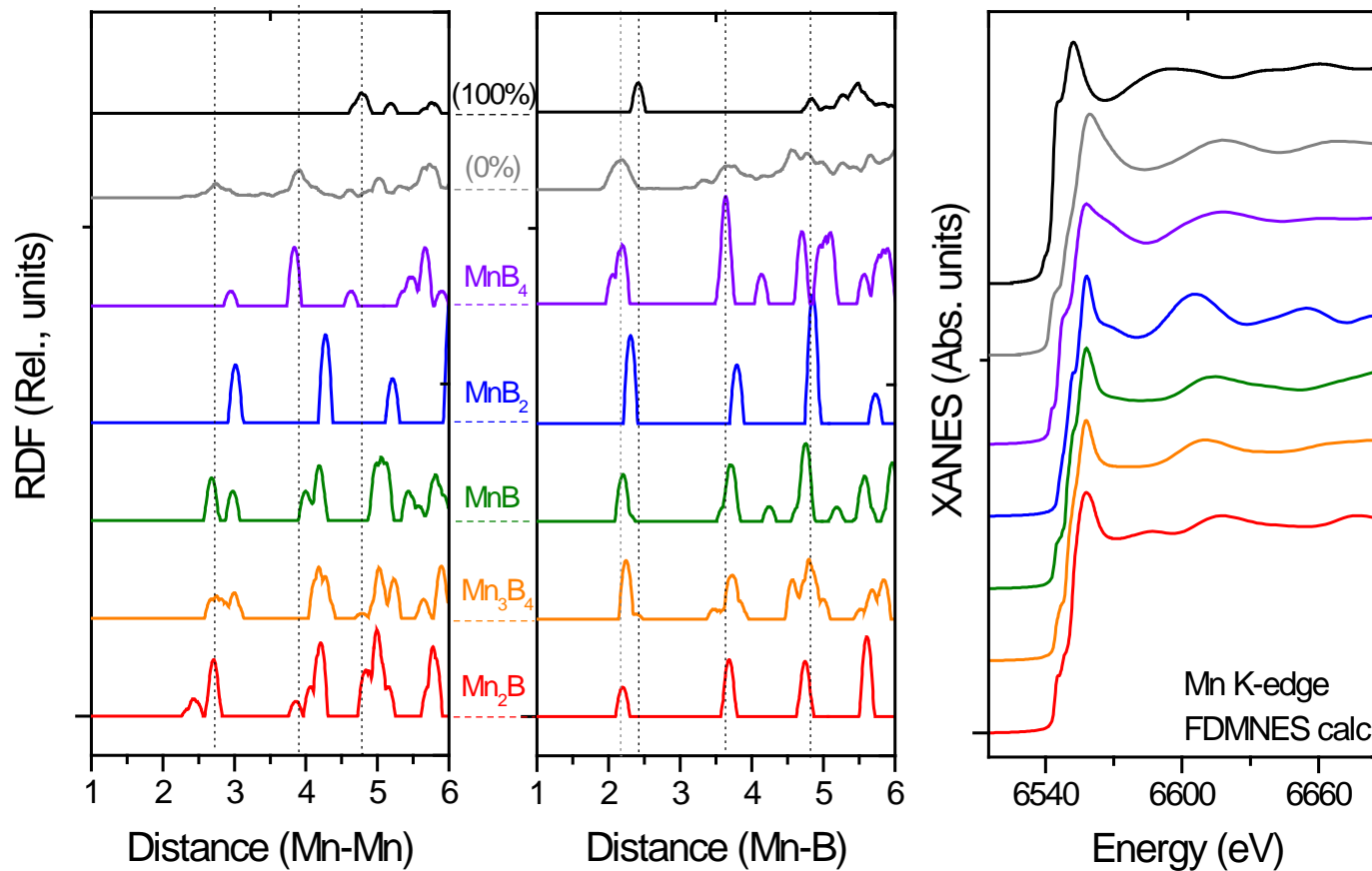
5) **It was assumed that the** sample after heating has **unhomogeneous structure** with a **nanodomain features** corresponding to various crystalline atomic ordering.

6) **Several** low-energy structural models were obtained by the mean of **evolutionary algorithm** implemented in **USPEX code**.

7) **XANES spectra** calculated for the relaxed structures in a good agreement with experimental data. This fact is approve a correctness of the result of geometry optimization.

**THANK YOU FOR ATTENTION!!!**

# Suppl. #1



# 13. USPEX: structure predictions

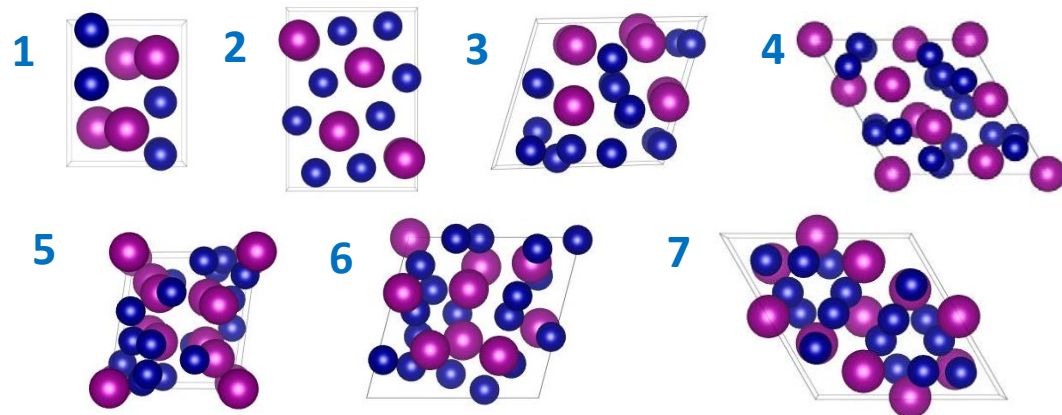


An accuracy of modeling is approved by XANES Mn K-edge spectra calculated for structural models predicted by the mean of Evolutionary algorithm which is implemented in USPEX code. The XANES spectra simulated for the more stable low-energy structures in a good agreement with the experimental curve obtained after heating the sample. Such a way we can conclude that interatomic distance and structural changes were determined correctly.

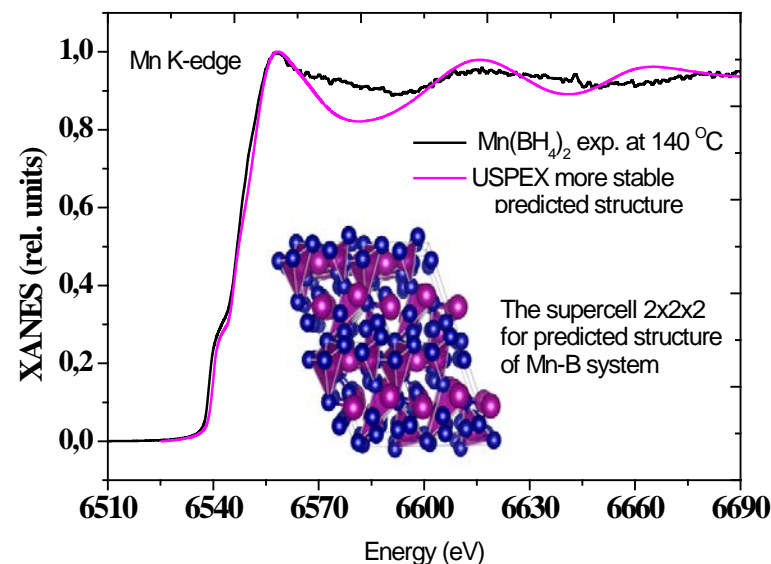
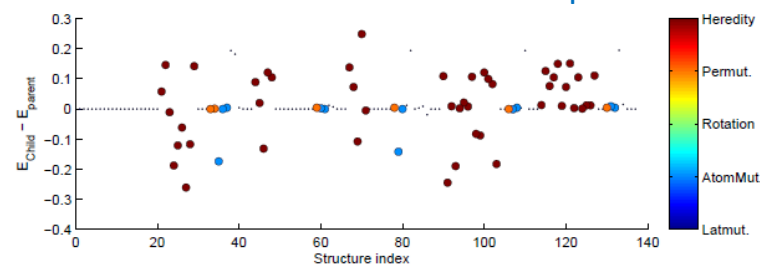
## Results of DFT-based modeling in comparison with the XRD.

Model	Mn-B distance (Å)	Mn-Mn distance (Å)	Cell volume
XRD. Mn(BH <sub>4</sub> ) <sub>2</sub> before heating	2,44 ± 0,02	4,81 - 0,01	1021,7
VASP. Before desorption (Model 1)	2,41 ± 0,01	4,77 ± 0,02	996,8
VASP. Partial desorption (Model 2)	2,28 ± 0,09	3,88 ± 0,24	643,6
VASP. After desorption (Model 3)	2,17 ± 0,05	2,72 ± 0,18	216,3
USPEX	2,08 - 2,14	2,59 - 2,88	206,4

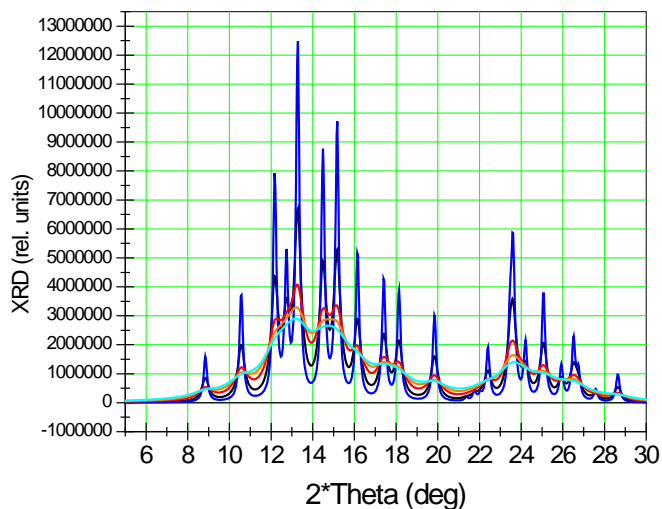
The most probable structural models for **Mn-B** systems predicted by means of **USPEX** algorithm:



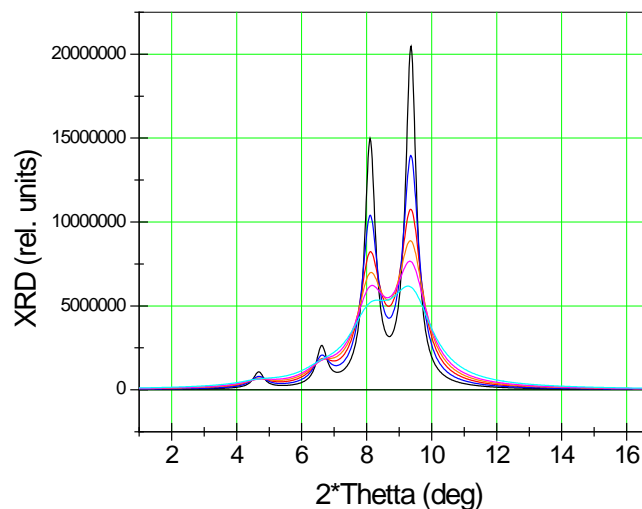
## Different kinds of variations operators



# Моделирование рентгеновских порошковых дифрактограмм XRPD



Моделирование XRD спектров для борида марганца MnB при различном значении параметра  $\gamma$



Моделирование XRD спектров для металлического марганца при различном значении параметра  $\gamma$

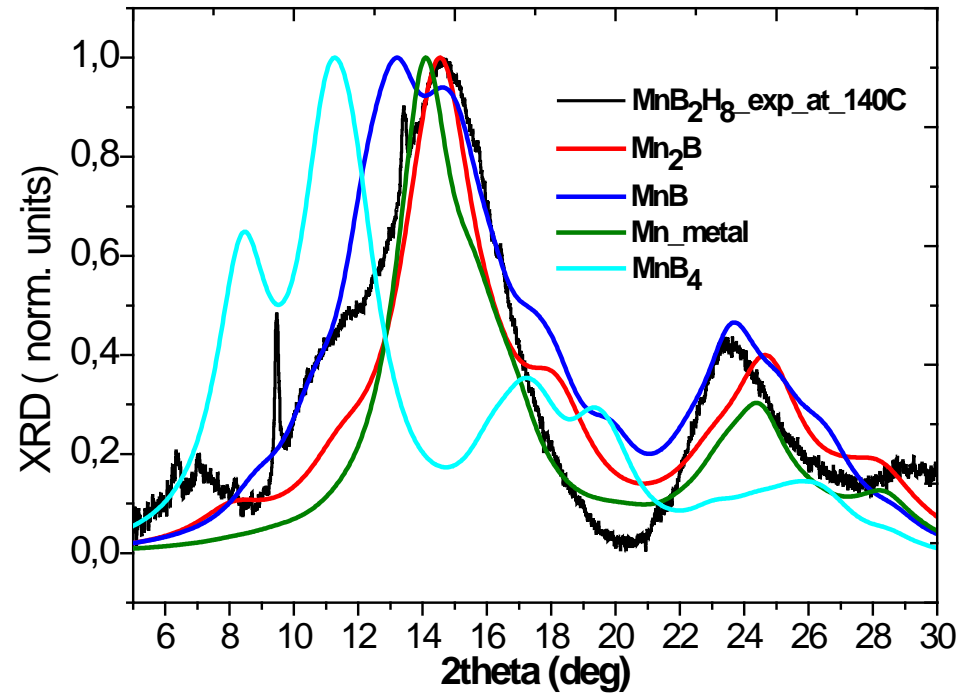
Расчетная формула для оптимизации ширины дифракционных пиков с целью учета их уширения в результате аморфизации исходного материала:

$$Int(\vartheta, \gamma) = \sum_{k=0}^n C \frac{I_k * \gamma}{(\vartheta - \vartheta_o^k)^2 + \gamma^2}$$

Где:

$I_k$  — значение интенсивности  $k$  — ого пика;  $\vartheta_o^k$  — угловая локализация;  $k$  — ого пика;  $C$  — нормировочная постоянная;  $\gamma$  — варьируемый параметр

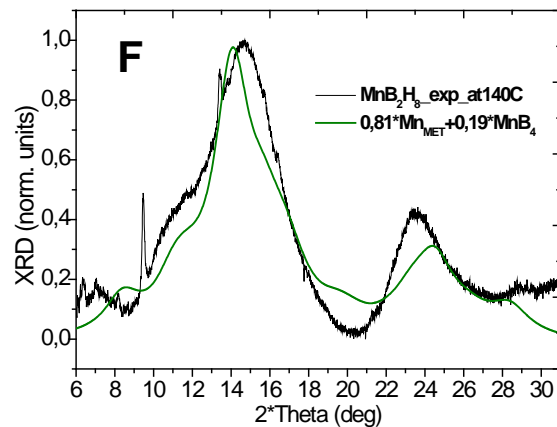
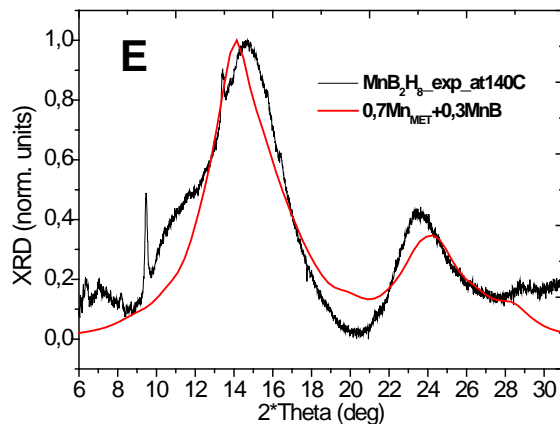
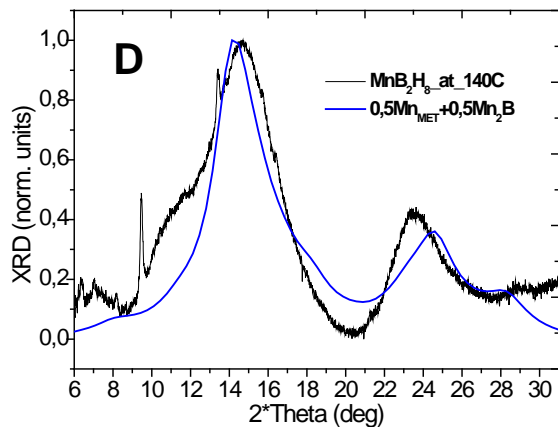
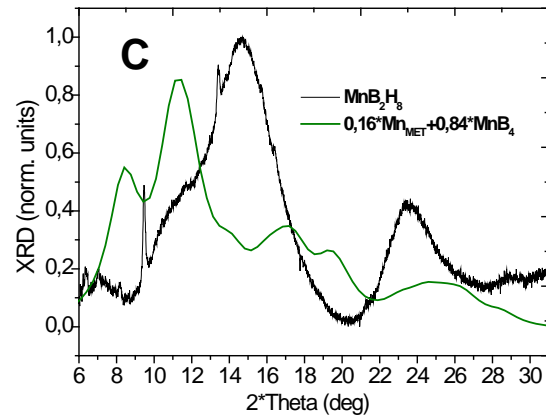
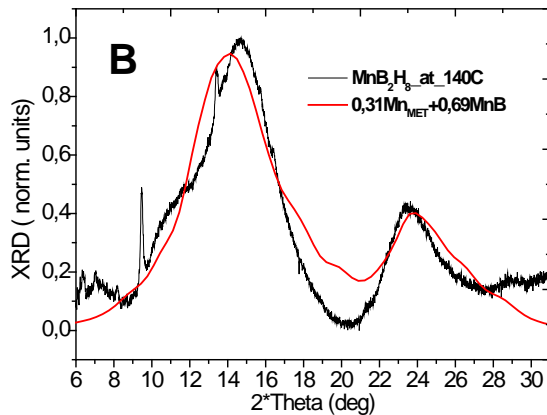
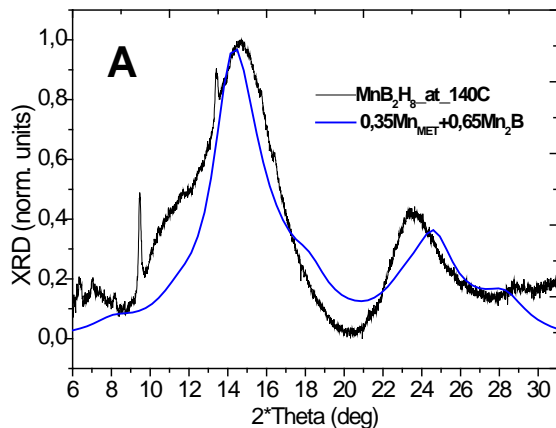
На следующем этапе была проведена оценка адекватности применяемой методики расчета. Также были смоделированы XRD спектры для возможных продуктов реакции разложения с учетом уширения дифракционных пиков.



Теоретически рассчитанный XRD спектр для борогидрида марганца  $MnB_2H_8$  в сравнение с экспериментальной кривой до десорбции водорода

Теоретическое моделирование XRD спектров для возможных продуктов реакции разложения исходного соединения  $MnB_2H_8$

# A,B,C - суперпозиция XRD спектров с весовыми коэффициентами полученными в результате фитинга спектров поглощения



D,E,F – суперпозиция XRD спектров с весовыми коэффициентами, полученными в результате фитинга рентгеновских дифрактограмм с учетом уширения пиков

# Определение размера наночастиц

Формула Шеррера позволяет оценить размер когерентности по дифракционным максимумам:

$$L = \frac{k\lambda}{\beta \cos \vartheta}$$

$k$  – форм фактор;

$\lambda$  – длина волны;

$\beta$  ( $FWHM$ ) – полная ширина на половине максимума;

$\vartheta$  – угловая локализация максимум

